IOP PUBLISHING JOURNAL OF PHYSICS A: MATHEMATICAL AND THEORETICAL

J. Phys. A: Math. Theor. **43** (2010) 354002 (9pp) doi:10.1088/1751-8113/43/35/354002

Asymptotics of the many-whirls representation for Aharonov–Bohm scattering

M V Berry

H H Wills Physics Laboratory, Tyndall Avenue, Bristol BS8 1TL, UK

Received 11 January 2010, in final form 22 February 2010
Published 12 August 2010
Online at stacks.iop.org/JPhysA/43/354002

Abstract
The previously derived decomposition of the Aharonov–Bohm (AB) wavefunction, into 'whirling waves' that wind different numbers of times round the flux line, is studied in detail. Asymptotic approximations are derived, describing many windings, far from the flux, and near the forward direction where the incident and scattered waves cannot be separated. The many-whirls representation gives insight into elementary explanations of the AB in terms of interference between waves passing on either side of the flux; three whirling waves suffice to give a very accurate description of the AB wave.

PACS numbers: 02.30.Mv, 03.65.Nk, 03.65.Vf

1. Introduction

In the Aharonov–Bohm (AB) effect [1–3], quantum waves representing a charged particle are scattered by a magnetic flux line that is inaccessible to them. This is often interpreted, and was so interpreted in a partial anticipation [4] of the AB effect, as interference between two waves travelling on either side of the flux, with the interference fringes shifted by Dirac's magnetic phase factor. But the interference picture is an approximation, with the deficiency that the wavefunction it implies is not singlevalued. Several decades ago, I showed [5] that the approximation can be corrected by including waves that have made more circuits of the flux line; the sum of these 'whirling waves' is singlevalued, and reproduces the exact AB wavefunction.

My purpose here is to make a more detailed study of the whirling waves in this 'many-whirls' representation. The formalism of [5] is summarized in section 2, with numerical calculations illustrating how the contributions from the higher–order windings get smaller. In section 3, the whirling waves are studied asymptotically, for large orders of winding, for large distance from the flux, and close to the forward direction where the incident and scattered waves cannot be separated. Finally, in section 4 the simple interference picture [4] is interpreted in terms of contributions from two whirling waves and a very accurate approximation is obtained with three whirling waves.

The treatment here will be restricted to the simplest AB wave, representing the idealized situation of scattering of a monochromatic plane wave from an infinitely thin line of flux. This

is not a serious restriction: as was shown before [5], the whirling-wave picture applies more widely, to describe how the flux modifies scattering and interference that exists even if there is no flux (e.g. from finite cylinders and in biprism experiments [6]).

2. Whirling-wave formulation

For flux Φ and incident particles with charge q, the quantum effects depend on the combination $\alpha = q\Phi/h$, in particular the fractional part

$$\alpha_{\rm fr} = \alpha - \mathrm{int}\,\alpha. \tag{2.1}$$

This reflects the precise identification by Wu and Yang [7] of the way in which observable quantum effects are underdetermined by classical electromagnetic fields: the extra information is in the gauge-independent phase factor $\exp(2\pi\,\mathrm{i}\alpha) = \exp(2\pi\,\mathrm{i}\alpha_{\rm fr})$. The integer part of α contributes an overall phase factor $\exp(\mathrm{i}\theta\mathrm{int}\alpha)$, which is unobervable in quantum mechanics but has been seen directly in water-wave analogue experiments [8].

In polar coordinates, the exact AB wavefunction [1], for a plane wave incident from $\theta = 0$ (i.e. $x = +\infty$) on a flux line of strength α at the origin, was derived by AB [1] as a sum over Bessel functions, representing contributions corresponding to different angular momenta l:

$$\psi = \psi(r,\theta;\alpha) = \sum_{l=-\infty}^{\infty} (-\mathrm{i})^{|l-\alpha|} J_{|l-\alpha|}(r)\exp(\mathrm{i}l\theta). \tag{2.2}$$

Here distance r is measured in units $1/\text{wavenumber} = \text{wavelength}/2\pi$, reflecting the absence of a separate length scale. From (2.2) follows the continuation rule

$$\psi(r,\theta;\alpha+1) = \exp(\mathrm{i}\alpha\theta)\psi(r,\theta;\alpha). \tag{2.3}$$

Therefore, it is necessary to consider only the range $0 \leqslant \alpha < 1$, and to simplify writing some formulas we apply this restriction from now on.

The standard technique for transforming sums over quantum numbers to sums over contributions representing different topologies is the Poisson summation formula [9]. It has been applied to waveguides [10], magnetic oscillations [11], rainbow scatttering [12–14], electron diffraction [15], and quantum chaos [16]. For the AB effect, the quantum number is l and the topologies, represented by an integer m, are the whirling waves with angular dependence $\theta+2\pi m$. In [5] the transformed wave was obtained as

$$\psi = \sum_{m=-\infty}^{\infty} \exp\{\mathrm{i}\alpha(\theta+2m\pi)\}T(r,\theta+2m\pi), \tag{2.4}$$

in which the individual whirling waves are

$$T(r,\theta) = \int_{-\infty}^{\infty} \mathrm{d}\lambda J_{|\lambda|}(r)\exp\left\{\mathrm{i}\left(\lambda\theta - \frac{1}{2}\pi\,|\lambda|\right)\right\}. \tag{2.5}$$

In (2.4) the individual contributions are not singlevalued, but the sum obviously is. An attractive feature of this representation is the explicit separation, in each of the whirling waves, of the magnetic phase factor involving the flux. An interpretation of (2.4) is that the AB wave lives on a Riemann surface corresponding to the angle variable θ extended to the full line $-\infty < \theta < +\infty$, with sheets corresponding to the subintervals $2\pi m \leqslant \theta < 2\pi\,(m+1)$. The physical AB wave can be regarded as a projection: the sum of waves on all the sheets. In the absence of flux ($\alpha = 0$), the whirling-wave decomposition is an unusual representation of the incident plane wave $\exp(-\mathrm{i}r\cos\theta)$.

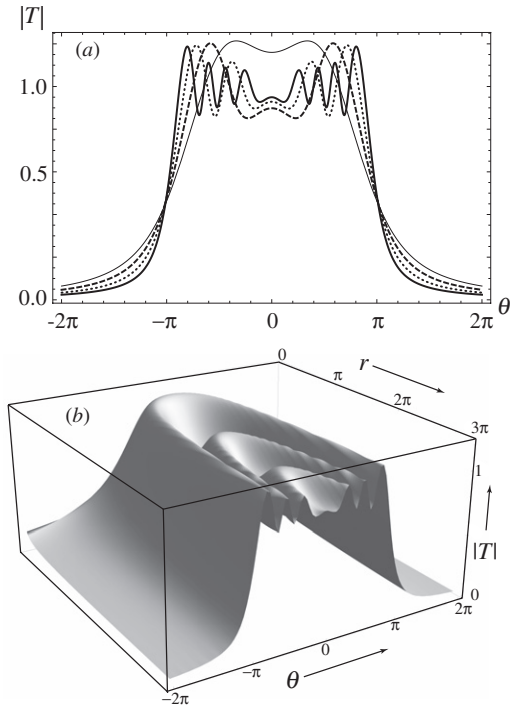

Figure 1. Modulus $|T(r,\theta)|$ of whirl function, showing decay outside the region $|\theta| \leqslant \pi$; (*a*) For $r = \pi/2$ (thin), π (dashed), 2π (dotted) and 4π (thick); (*b*) 3D plot.

In (2.5), the Bessel functions decay rapidly for $|\lambda| > r$, so the integral is easy to evaluate numerically. Figure 1 illustrates how $|T(r,\theta)|$ gets smaller as θ gets farther from the interval $-\pi < \theta < \pi$, that is for more windings m in (2.4). This justifies the approximation of the AB effect in terms of a few interfering waves, as will be explained in more detail in section 4.

Formula (2.5) for the whirling waves is not convenient for the analytical explorations to follow. Instead we will use a different expression, stated without proof in [5], and here derived in the appendix:

$$T(r,\theta+2\pi m) = \exp(-\mathrm{i}r\cos\theta)\delta_{m,0} - \frac{1}{\pi}\int_{-\infty}^{\infty}\mathrm{d}y\,\frac{(\pi+\mathrm{i}y)\exp(\mathrm{i}r\cosh y)}{(\pi+\mathrm{i}y)^2-(\theta+2\pi m)^2} \quad (|\theta|\leqslant\pi). \tag{2.6}$$

The integral converges rapidly if the contour is deformed to $-\infty - \frac{1}{2}\mathrm{i}\pi < y < \infty + \frac{1}{2}\mathrm{i}\pi$.

Although the singlevalued sum ψ is a smooth periodic function of θ, the individual whirling waves, labelled by m, are discontinuous in the forward direction $\theta = \pm\pi$. This is illustrated in figure 2, which also illustrates the higher whirling waves getting smaller, as will be described analytically in the following section.

By evaluating the sum in (2.4), formula (2.6) leads to the following integral representation for the AB wave, which, although we will not make use of it, is interesting:

$$\psi = \exp(-\mathrm{i}r\cos\theta+\mathrm{i}\alpha\theta) - \frac{\sin(\pi\alpha)}{\pi}\exp\{\mathrm{i}\alpha\theta\} \times\int_{-\infty}^{\infty}\mathrm{d}y\exp(\mathrm{i}r\cosh y)\frac{(\exp(\mathrm{i}\theta)\cosh(\alpha y)+\cosh((\alpha-1)y))}{\cosh y+\cos\theta} \quad (0\leqslant|\theta|\leqslant\pi). \tag{2.7}$$

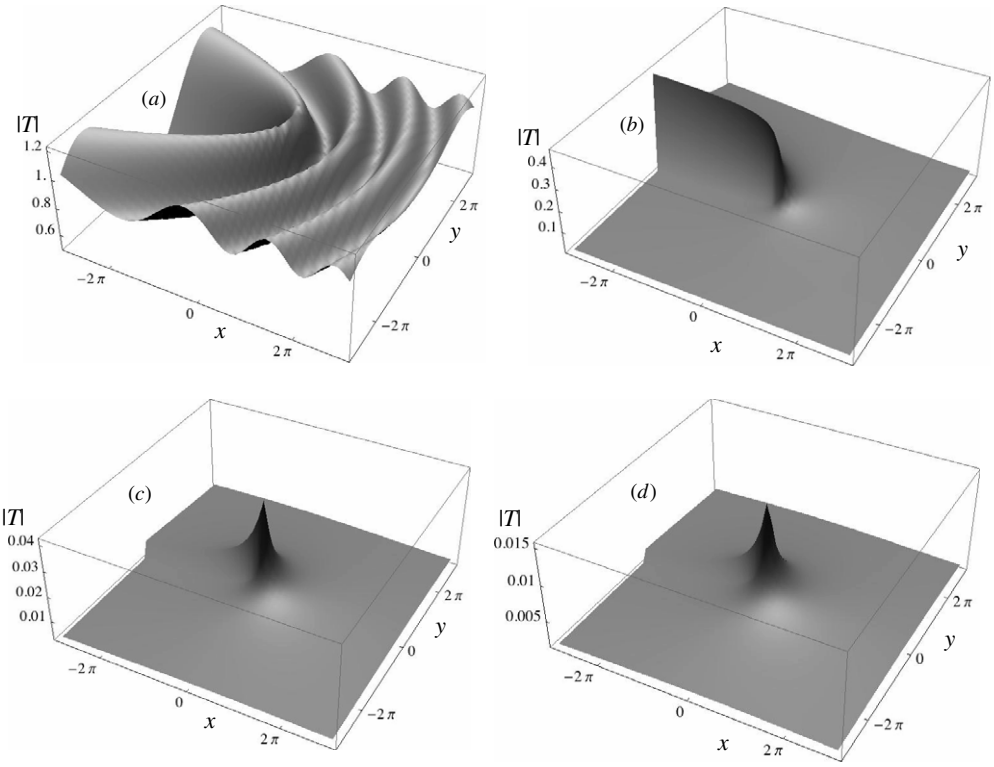

Figure 2. Modulus of individual whirling waves in cartesian coordinates, that is $|T(r=\sqrt{x^2+y^2}, \theta = \arg(x+\mathrm{i}y)+2m\pi)|$, for (a) $m=0$, (b) $m=-1$, (c) $m=-2$, (d) $m=-3$ (the whirling waves for positive m are identical except that y is replaced by $-y$).

3. Whirl asymptotics

For the high-order whirls, (2.6) gives, in terms of the outgoing Hankel function

$$T(r,\theta+2\pi m) \approx \frac{2}{(2\pi m+\theta)^2}\int_0^\infty \mathrm{d}y\,\exp(\mathrm{i}r\cosh y)$$
$$= \frac{\mathrm{i}\pi}{(2\pi m+\theta)^2}H_0^{(1)}(r) \quad (|m|\gg 1). \tag{3.1}$$

This shows that the whirl series converges as $1/m^2$.

For $r >> 1$, that is many wavelengths from the flux line, the integrand in (2.6) oscillates rapidly, and the main contribution comes from the stationary point at $y=0$. Elementary application of the method of stationary phase gives

$$T(r,\theta+2\pi m) \approx \exp(-\mathrm{i}r\cos\theta)\delta_{m,0} - \sqrt{\frac{2\pi\mathrm{i}}{r}}\frac{\exp(\mathrm{i}r)}{(\pi^2-(\theta+2\pi m)^2)}$$
$$(r\gg 1, 0\leqslant|\theta|\leqslant\pi). \tag{3.2}$$

This formula and (3.1) overlap in their common range of validity, i.e. r and $|m|$ large.

All the whirling waves except the incident-wave contribution to $m=0$ radiate outwards, as they must since the AB wave represents scattering by the flux. The sum of all the contributions

(3.2) gives an alternative derivation of the far-field AB scattering amplitude $f(\theta)$ obtained originally [1], namely

$$\psi \approx \exp(-\mathrm{i}r\cos\theta + \mathrm{i}\alpha\theta) + \frac{f(\theta)}{\sqrt{r}}\exp(\mathrm{i}r), \tag{3.3}$$

where

$$f(\theta) = -\sqrt{\frac{\mathrm{i}}{2\pi}}\frac{\sin(\pi\alpha)}{\cos\left(\frac{1}{2}\theta\right)}\exp\left(\frac{1}{2}\mathrm{i}\theta\right). \tag{3.4}$$

In the forward direction $\theta = \pm\pi$, this scattering amplitude, and the whirling-wave large r expressions (3.2) for $m = 0$ and $m = \pm 1$, diverge. This reflects the well-known inability to separate the incident and scattered fields in the forward direction. Indeed, the stationary phase approximation of (3.2) fails for $\theta = \pm\pi$, because in (2.6) a pole of the integrand coincides with the stationary point as $\theta \to \pm\pi$. To incorporate this feature, and thereby derive a version of (3.2), that is valid close to the forward direction, we first consider the case $m = 0$.

First, we write (2.6) as

$$T(r,\theta) = \exp(-\mathrm{i}r\cos\theta) - \frac{1}{2\pi}\int_{-\infty}^{\infty}\mathrm{d}y\exp(\mathrm{i}r\cosh y)\left(\frac{1}{\pi + \mathrm{i}y - \theta} + \frac{1}{\pi + \mathrm{i}y + \theta}\right) \quad (|\theta| \leqslant \pi). \tag{3.5}$$

At $\theta = \pi$ ($\theta = -\pi$) the first (second) factor in the parenthesis has a pole, For large r, the main contribution to each integral comes from the stationary point at $y = 0$, so we can approximate $\cosh y \approx 1 - \frac{1}{2}y^2$. The integral without a pole can be approximated by stationary phase, and the integral with a pole can be evaluated in terms of the complementary error function. A short calculation leads to

$$T(r,\theta) \approx \exp(-\mathrm{i}r\cos\theta) - \frac{\exp\left\{\mathrm{i}\left(r + \frac{1}{4}\pi\right)\right\}}{\sqrt{2\pi r}\,(\pi + |\theta|)} - \frac{\exp\left\{\mathrm{i}r\left(1 - \frac{1}{2}(\pi - |\theta|)^2\right)\right\}}{2}\mathrm{Erfc}\left(\exp\left(-\frac{1}{4}\mathrm{i}\pi\right)\sqrt{\frac{r}{2}}(\pi - |\theta|)\right) \quad (-\pi \leqslant \theta \leqslant \pi). \tag{3.6}$$

The Erfc function gives a significant modification to (3.2) in the near-forward intervals $\pi - |\theta| < 1/\sqrt{r}$, where, as is already known [8], the incident and scattered waves cannot be separated. Outside these intervals, Erfc can be approximated by its large-argument asymptotic approximation, and (3.6) reduces to (3.2). As figures 3(*b*) and (*c*) illustrate, (3.6) is an extraordinarily accurate approximation, uniformly valid over the whole angular range, even very close to the flux line (in figure 3(*c*), $r = 1 = \text{wavelength}/2\pi$).

However, (3.6) is not quite smooth; the dependence on $|\theta|$ signals a discontinuity of slope in the backward direction $\theta = 0$, arising from the first correction to the leading-order asymptotics of Erfc. This is very weak: the slope at $\theta = 0$ is smaller than that at $\theta = \pm\pi$ by a factor $\sqrt{2}/\pi^{7/2}r^{3/2}$—invisible in figure 3(*c*) and barely discernible for $r = 0.5$, which is only $1/4\pi$ wavelengths from the flux.

For $m = \pm 1$, a similar argument gives the uniform approximations

$$T(r,\theta \pm 2\pi) \approx -\frac{\exp\left\{\mathrm{i}\left(r + \frac{1}{4}\pi\right)\right\}}{\sqrt{2\pi r}(3\pi \pm \theta)} + \frac{\exp\left\{\mathrm{i}r\left(1 - \frac{1}{2}(\pi \pm \theta)^2\right)\right\}}{2}\mathrm{Erfc}\left(\exp\left(-\frac{1}{4}\mathrm{i}\pi\right)\sqrt{\frac{r}{2}}(\pi \pm \theta)\right) \quad (-\pi \leqslant \theta \leqslant \pi). \tag{3.7}$$

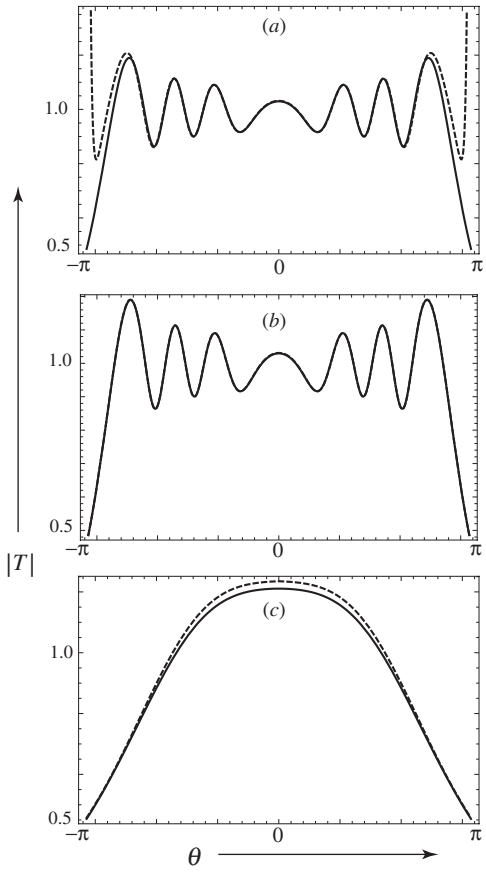

Figure 3. Full curves: $|T(r,\theta)|$ for (*a*), (*b*) $r = 10$, (*c*) $r = 1$. Dashed curves: (*a*) large r approximation (3.2), (*b*), (*c*) uniform approximation (3.6) (in (*b*) the two curves are indistinguishable).

In both cases, $|T|$ decays monotonically away from the forward direction, that is θ increasing from $-\pi$ for $T(r, \theta + 2\pi)$, and θ decreasing from π for $T(r, \theta - 2\pi)$.

The error function with argument proportional to $\exp(-i\pi/4)$ can be expressed in terms of the Fresnel sine and cosine integrals, represented geometrically in terms of the Cornu spiral. In AB theory these integrals were originally noticed for the special case $\alpha = 1/2$ [1], and the Cornu spiral is the basis of a very accurate approximation for all α [17], different from the whirling-wave deomposition studied here.

4. Ehrenberg–Siday approximation

Elementary accounts of the AB effect, starting with the partial anticipation by Ehrenberg and Siday (ES) [4], commonly consider the incident wave split into two halves, passing different ways round the flux line and accumulating different magnetic phase factors, that are then recombined and interfere. For the idealized situation considered here, where there is no

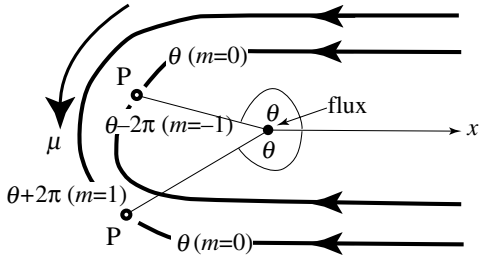

Figure 4. Waves at points P after passing above and below the flux, leading to the wave (4.1).

interference without flux, the superposition is (cf figure 4)

$$\psi\,(r,\theta) \approx \tfrac{1}{2}\exp\left(-\mathrm{i}r\cos\theta + \mathrm{i}\alpha\theta\right) + \tfrac{1}{2}\exp\left(-\mathrm{i}r\cos\theta + \mathrm{i}\alpha\,(\theta - 2\pi\,\mathrm{sgn}\theta)\right)$$
$$= \exp(\mathrm{i}r\cos\mu + \mathrm{i}\alpha\mu)\cos\pi\alpha \quad (-\pi \leqslant \theta \leqslant \pi), \tag{4.1}$$

where $\mu = \theta\text{-}\pi\,\mathrm{sgn}\theta$ is a coordinate varying smoothly through the forward direction $\mu = 0$.

The factor $\cos\pi\alpha$ captures the AB interference in a rudimentary form, but the intensity of the approximate wave (4.1) is constant. Worse, it is obvious that this wave must be multivalued: in the form written, it is discontinuous in the backward direction $x > 0$, corresponding to the incident wave (figure 5(*a*)). This corresponds to the situation in many interferometers, where the incident wave is split into two, but in every interferometer the wave must be singlevalued in the full space (an observation with interesting consequences [18]). Usually it is hard to write the singlevalued wave explicitly, but this was achieved for the AB wave with the function (2.2).

Figure 5(*b*) shows the exact AB wavefunction. Clearly, the approximation (4.1) captures little of its richness. But the whirling-wave decomposition described earlier [5], and elaborated here, can build on the insight embodied in (4.1), by representing ψ as the sum (2.4) over a few windings. The simplest approximation capturing the behaviour near the forward direction involves the whirling waves $m = 0, 1, -1$, namely

$$\psi \approx T(r,\theta)\exp\{\mathrm{i}\alpha\theta\} + T(r,\theta+2\pi)\exp\{\mathrm{i}\alpha(\theta+2\pi)\}$$
$$+ T(r,\theta-2\pi)\exp\{\mathrm{i}\alpha(\theta-2\pi)\} \quad (-\pi \leqslant \theta \leqslant \pi). \tag{4.2}$$

The term $m = +1$ corrects the wave near $\theta = -\pi$, and the term $m = -1$ corrects the wave near $\theta = +\pi$. With the exact whirling waves (2.5) or (2.6), these three contributions give a very accurate description, for example a picture indistinguishable from the exact AB wave in figure 5(*b*). The same is true if the whirling waves in (4.2) are replaced by the uniform approximations (3.6) and (3.7).

Of course these approximations must fail somewhere. Already mentioned is the weak discontinuity for $x > 0$, in the slope of the uniform approximation (3.6) for $m = 0$. Truncation of the whirling-wave sum at $|m| = 1$ introduces a discontinuity in the value of ψ itself in the forward direction $x < 0$. This is very weak, and decays with increasing r: asymptotically, the jumps in ψ and the modulus $|\psi|$ are

$$\psi(r,\pi) - \psi(r,-\pi) \approx \mathrm{i}\frac{\sin(3\pi\alpha)}{(2\pi)^{3/2}\sqrt{r}}\exp\left\{\mathrm{i}\left(r + \frac{1}{4}\pi\right)\right\},$$
$$|\psi\,(r,\pi)| - |\psi\,(r,-\pi)| \approx \frac{\sin(3\pi\alpha)}{4\,(\pi)^{3/2}\sqrt{r}}. \tag{4.3}$$

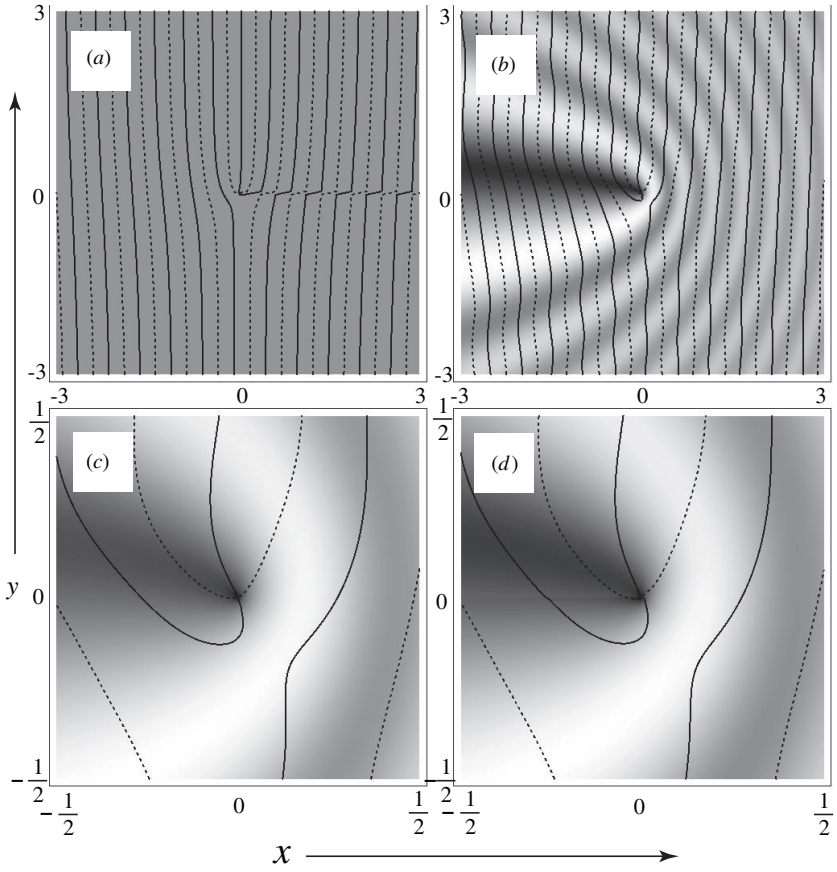

Figure 5. Modulus (grayscale) and wavefronts (phase contours) of the AB wave ψ for flux $\alpha = 0.75$, corresponding to a plane wave incident from $x = +\infty$; the full curves represent $\arg\psi = (0 \text{ and } \pi)$, dashed curves represent $\arg\psi = \pm\pi/2$, and distances are labelled in wavelength units. (*a*) simple interference approximation (4.1); (*b*) exact AB wavefunction (2.2); (*c*) magnification of (*b*); (*d*) representation in terms of three whirling waves (4.3), approximated uniformly by (3.6) and (3.7). In (*d*) the discontinuity in the forward direction ($x < 0$) is barely discernible.

To see the jumps, it is necessary to look close to the flux line. Even then, they can barely be seen: compare figure 5(*c*), which is a magnification of the exact AB wave in figure 5(*a*), with the three-whirl approximation in figure 5(*d*). The jump in the forward direction can be reduced by incorporating the higher whirls $|m| = 2,3\ldots$, and of course disapppears when all windings are included.

Acknowledgments

I thank Tel Aviv University for hospitality during the Aharonov–Bohm effect 50th anniversary meeting, where this work was begun. My research is supported by the Leverhulme Trust.

Appendix. Derivation of whirling-wave expression (2.6)

Beginning with (2.5), the first step is to replace the Bessel functions by the integral representation

$$J_{|\lambda|}(r) = \frac{\exp\left(\frac{1}{2}\pi\,|\lambda|\right)}{2\pi}\int_C \mathrm{d}s\,\exp\{\mathrm{i}(|\lambda|s - r\cos s)\}, \tag{A.1}$$

where C is the contour $\{\mathrm{i}\infty - \pi, -\pi, \pi, \pi + \mathrm{i}\infty\}$ infinitesimally shifted to the left. Writing the whirl index explicitly gives, from (2.5)

$$\begin{aligned} T(r, \theta + 2\pi m) &= \frac{1}{2\pi}\int_C \mathrm{d}s\,\exp(-\mathrm{i}r\cos s)\int_{-\infty}^{\infty}\mathrm{d}\lambda\,\exp\{\mathrm{i}\,(|\lambda|\,s + \lambda\,(\theta + 2\pi m))\} \\ &= \frac{\mathrm{i}}{\pi}\int_C \mathrm{d}s\,\exp(-\mathrm{i}r\cos s)\frac{s}{s^2 - (\theta + 2\pi m)^2} \quad (|\theta| \leqslant \pi). \end{aligned} \tag{A.2}$$

For the leg of C on the real axis, the contributions for all $m \neq 0$ vanish because the integrand is odd, and for $m = 0$ there are contributions from poles at $s = \pm\theta$. For the vertical legs, we write $s = \pm\pi + \mathrm{i}y$, and combine the two integrals into a single integral over the interval $-\infty < y < +\infty$. These observations lead directly to (2.6).

References

[1] Aharonov Y and Bohm D 1959 Significance of electromagnetic potentials in the quantum theory *Phys. Rev.* **115** 485–91

[2] Olariu S and Popescu I I 1985 The quantum effects of electromagnetic fluxes *Rev. Mod. Phys.* **57** 339–436

[3] Peshkin M and Tonomura A 1989 *The Aharonov–Bohm Effect Springer Lecture Notes in Physics 430* (Berlin: Springer)

[4] Ehrenberg W and Siday R E 1949 The refractive index in electron optics and the principles of dynamics *Proc. Phys. Soc.* B **62** 8–21

[5] Berry M V 1980 Exact Aharonov–Bohm wave function obtained by applying Dirac's magnetic phase factor *Eur. J. Phys.* **1** 240–4

[6] Chambers R G 1960 Shift of an electron interference pattern by enclosed magnetic flux *Phys. Rev. Lett.* **5** 3–5

[7] Wu T T and Yang C N 1975 Concept of nonintegrable phase factors and global formulation of gauge fields *Phys. Rev.* D **12** 3845–57

[8] Berry M V, Chambers R G, Large M D, Upstill C and Walmsley J C 1980 Wavefront dislocations in the Aharonov–Bohm effect and its water-wave analogue *Eur. J. Phys.* **1** 154–62

[9] Lighthill M J 1958 *Introduction to Fourier Analysis and Generalized Functions* (Cambridge: Cambridge University Press)

[10] Pekeris C L 1950 Ray theory vs normal mode theory in wave propagation problems *Proc. Symp. Appl. Math.* **2** 71–5

[11] Lifshitz E M and Pitaevskii L P 1980 *Statistical Physics Part 2: Landau and Lifshitz Course of Theoretical Physics* vol 9 (Oxford: Heinemann)

[12] Berry M V 1966 Uniform approximation for potential scattering involving a rainbow *Proc. Phys. Soc.* **89** 479–90

[13] Berry M V and Mount K E 1972 Semiclassical approximations in wave mechanics *Rep. Prog. Phys.* **35** 315–97

[14] Nussenzveig H M 1992 *Diffraction Effects in Semiclassical Scattering* (Cambridge: Cambridge University Press)

[15] Berry M V 1971 Diffraction in crystals at high energies *J. Phys. C: Solid State Phys.* **4** 697–722

[16] Berry M V and Tabor M 1976 Closed orbits and the regular bound spectrum *Proc. R. Soc.* A **349** 101–23

[17] Berry M V and Shelankov A 1999 The Aharonov-Bohm wave and the Cornu spiral *J. Phys. A: Math. Gen.* **32** L447–55

[18] Berry M V 2007 Wave dislocations threading interferometers *Proc. R. Soc.* A **463** 1697–711